applied sciences

MDPI

Article

First Observations of Cirrus Clouds Using the UZ Mie Lidar over uMhlathuze City, South Africa

Nkanyiso Mbatha [1] and Lerato Shikwambana [2,*]

[1] Department of Geography, University of Zululand, KwaDlangezwa 3886, South Africa; mbathanb@unizulu.ac.za
[2] Earth Observation Directorate, South African National Space Agency, Pretoria 0001, South Africa
* Correspondence: lshikwambana@sansa.org.za

Abstract: Clouds cover more than two-thirds of the earth's surface and play a dominant role in the energy and water cycle of our planet. Cirrus clouds are high-level clouds composed mostly of ice crystals and affect the earth's radiation allocation mainly by absorbing outgoing longwave radiation and by reflecting solar radiation. This study presents the characterization of cirrus clouds observed on 10 and 11 April 2019 using the ground-based University of Zululand (UZ) light detection and ranging (lidar) for the first time. Dense cirrus clouds with an average thickness of ~1.5 km at a height range of 9.5–12 km on 10 and 11 April 2019 were observed by the UZ lidar. The UZ lidar observation on 10 April 2019 agreed with the Cloud–Aerosol Lidar with Orthogonal Polarization (CALIOP) observation.

Keywords: lidar; cirrus clouds; CALIPSO; cloud optical depth; extinction coefficient

Citation: Mbatha, N.; Shikwambana, L. First Observations of Cirrus Clouds Using the UZ Mie Lidar over uMhlathuze City, South Africa. *Appl. Sci.* **2022**, *12*, 4631. https://doi.org/10.3390/app12094631

Academic Editors: Mikhail Vorontsov and Steve Hammel

Received: 4 February 2022
Accepted: 29 April 2022
Published: 5 May 2022

1. Introduction

Cirrus clouds are upper troposphere and lower stratosphere atmospheric clouds that have attracted much attention over the years due to their impact on the earth's radiation budget and thus climate [1,2]. The microphysical and optical properties of cirrus clouds are known to cause a warming effect in the tropics and a cooling effect at mid-latitudes [2,3]. Furthermore, cirrus clouds can be the platform for the genesis of heterogeneous reactions that influence the ozone budget in the lower stratosphere.

In general, clouds in the atmosphere are composed of hydrometeors that differ in phase, size, and shape. Hydrometeors in the atmosphere are mainly water droplets, ice crystals, raindrops, graupel, hail, and snowflakes [4]. Depending on the vertical temperature profile, the different hydrometeors can be present in all clouds in a more or less distinct number concentration.

Clouds cover more than two-thirds of the earth's surface and play a dominant role in the energy and water cycle of our planet [5,6]. The net cloud radiative effect on the climate system depends on the amount, height, and optical depth of clouds. Low-level clouds tend to be relatively thick optically and are typically composed of spherical water droplets, and their overall impact is to cool the planet. On the other hand, high-level clouds are optically thin and are composed mostly of ice crystals, with a wide variety of shapes and sizes, and their overall impact is to warm the planet.

Clouds are also an essential variable in the climate system because they are directly associated with precipitation through microphysical processes and with aerosol loading through the aerosol aqueous-phase chemistry and wet removal process [4]. Physically, cloud-radiation interactions depend largely on the cloud's macrophysical (e.g., cloud fraction, liquid and ice water path) and microphysical (e.g., cloud droplet number, size, and ice particle habit) properties.

The Cloud–Aerosol Lidar and Infrared Pathfinder Satellite Observations (CALIPSO) has been in orbit since 2006 and has been used to study the local and global spatial

distributions and heights of clouds. One of the advantages of CALIPSO is its capability to detect thin cirrus clouds. The high-quality vertical backscattering coefficients and depolarization ratio measurements are used to derive the vertical structure and properties of thin clouds [7]. Because of the sensitivity to very thin cirrus clouds, i.e., subvisible cirrus clouds with an optical depth of about 0.01, CALIPSO can provide information on multiple cloud layers. Furthermore, the light detection and ranging (lidar) instrument has also proven to be amongst the most effective instruments in studying and improving our understanding of cirrus clouds. One of the most important parameters is the lidar ratio (LR), i.e., extinction to backscattering ratio. LR depends on several characteristics of the particles, including their shape, size distribution, and refractive index [8]. Therefore, LR can provide indications about the ice-crystal characteristics [9]. Therefore, this makes lidars vital in studying cirrus clouds. Several authors [10,11] have used lidars to study cirrus clouds. More recently, the University of Zululand (UZ) (28.85° S, 31.84° E) installed and commissioned a Mie lidar system that is operated to measure clouds and aerosols.

In contrast to other continents, the UZ lidar is one of the only two lidars that are available in Africa and, at present, is the only one operational. UZ is situated in the Empangeni/Richards Bay (uMhlathuze City), a city that is highly industrialized [12]. This study area is also situated at the center of the sugarcane fields of KwaZulu Natal Province of South Africa. The sugarcane fields are owned by both large commercial companies and partly owned by local communities. The area is also dominated by sugar mills. More importantly is that the instrument is used to measure emissions during the harvest season when harvesters first burn sugar cane before curing it, which greatly tempers the air quality of the area and its surrounding. Thus, apart from the Highveld area of South Africa, which is known for its air quality issues, the study area where the lidar is situated, is an area that requires attention when it comes to accurate measurements of atmospheric chemistry and composition. However, due to the lack of funding for projects that can accurately probe the atmosphere in this study area, little or no studies have been performed in order to investigate the air quality of this study area. Thus, this lidar is strategically placed in this area for this reason. The other plan is to use the lidar data to calibrate the performance of satellite measurements in this area and also submit the data for use in reanalysis products and models.

This case study, though, came about because of the capabilities of this lidar to detect even activities in the upper troposphere and lower stratosphere. In terms of the use of the UZ lidar for cirrus clouds observations over South Africa, this is very important research because, in terms of the meteorology of South Africa, cirrus clouds are known to form from the ascent of dry air, which makes the small quantity of water vapor in the air undergo deposition into ice, which means it solidifies directly. The South African Weather Services (SAWS) use the sighting of the cirrus clouds as an indicator of the arrival of a warm front as the air masses meet at high levels, which indicates that a change in the weather is on the way. For many years, pictures have been used to profile these cirrus clouds. However, an instrument such as lidar is always a better option for the purpose of profiling these cirrus clouds because it can provide detailed characteristics of these clouds very accurately. Thus, cirrus clouds are important for the context of South Africa because the meteorology of this part of the world is heavily influenced by pressure systems. Apart from using the UZ lidar for air quality and cloud studies, another plan is to modify and use the UZ lidar for investigating the thermal structure over this region. Other similar have been conducted by Comerón et al. [13], Winker et al. [14], and Nellore and Kannan [15].

The study presents for the first time the observation of cirrus clouds based on two successive nights (10 and 11 April 2019) by the UZ lidar system. The UZ lidar results are further compared with CALIPSO observations. In particular, the study aims at determining the cloud properties such as cloud optical depth (COD), cloud position, occurrence height, backscatter coefficient and extinction coefficients.

2. Study Site

The Mie lidar is installed into a container and is deployed at the Universality of Zululand, South Africa. The University of Zululand is situated ~30 km south-west of the Richards Bay town (28.78° S, 32.03° E) which lies east of South Africa (see Figure 1). This city lies 121 m above sea level and is surrounded by forests. According to the Köppen–Geiger climate classification of South Africa [16], this city can be classified as having cool summers, being fully humid, and having an equatorial climate.

Figure 1. Map of South Africa with the location of the study area. The University of Zululand is located in the south-west of Richards Bay.

3. Methods and Data

3.1. UZ Lidar

The ground-based lidar system was commissioned at UZ in 2018 with the purpose of studying the vertical distribution of aerosols and clouds over the area. The UZ lidar has the same specification as the previously reported lidar system by Sharma [17], and the specifications are summarized in Table 1. The lidar system is made up of three sections, namely the transmission, receiver, and data acquisition, as seen in Figure 2.

Table 1. UZ lidar specification.

Parameter	
Wavelength	532 nm: Nd: YAG
Maximum pulse energy	160 mJ
Telescope	404 cm
Detector	PMT
Field of View	500 µrad
Vertical and temporal resolutions	10 m and 10 s

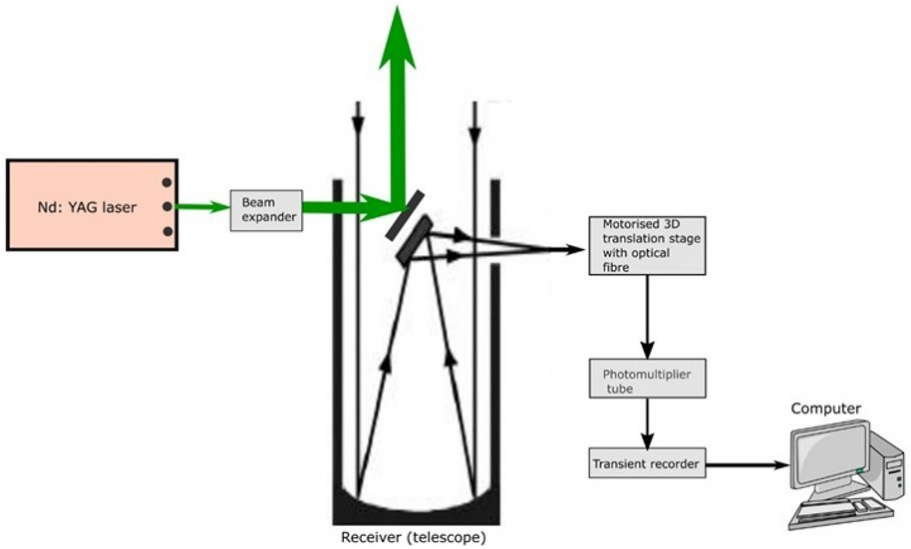

Figure 2. Schematic diagram for UZ lidar system.

The lidar measurements were carried out on 10 and 11 April 2019 in the early evenings until the night. The UZ lidar has the capability to operate during the day or night. However, because the overpass of CALIPSO over the Empangeni region is during the night, the UZ lidar was operated during the night to be able to compare UZ lidar and CALIPSO retrievals. The backscattered photons from the atmosphere were collected by the telescope, and the backscatter coefficient, extinction coefficient, and COD were retrieved using an analytical method.

The received intensity, $I(r)$ in terms of photon counts, is obtained over 256 range bins with a pulse width of 7 ns which is provided by the standard LIDAR equation [18] as

$$I(r) = I_0 C \beta(r) r^{-2} e^{-2\int_0^r \sigma(r\prime) dr\prime} \quad (1)$$

where I_0 is the transmitted laser intensity in terms of photon counts at 532 nm, C is the system constant, $\beta(r)$ is the backscattering coefficient, $\sigma(r)$ is the extinction coefficient and r is the range. The system constant C is provided by

$$C = \frac{\eta A_r c \tau}{2} \quad (2)$$

where η is efficiency of receiver system, A_r is receiving telescope area, c is the speed of light and τ is the pulse width of the transmitted laser beam. The single-wavelength lidar equation has two unknowns and can then be solved assuming proportionality between extinction and backscatter. The backscattering and extinction coefficients are provided by contribution of both aerosols and molecules and are expressed as:

$$\beta(r) = \beta_{aer}(r) + \beta_{mol}(r) \quad (3)$$

$$\sigma(r) = \sigma_{aer}(r) + \sigma_{mol}(r) \quad (4)$$

where subscript *(aer)* and *(mol)* indicate aerosols/clouds and molecules, respectively. Molecular contributions were calculated by taking data from MSIS-E-90 Atmosphere Model. The molecular backscatter coefficient $\beta_{mol}(r)$ is estimated by considering the theoretical molecular lidar ratio $S_{mol} = \frac{\sigma_{mol}}{\beta_{mol}}$ as $\frac{8\pi}{3}$ sr, under the condition of zero molecular absorption [18]. The total backscatter coefficients are derived from the backward inversion method and can be expressed as,

$$\beta_{aer}(r) + \beta_{mol}(r) = \frac{X(r)\ exp[-2(S_{aer}(r) - S_{mol})] \int_{r_c}^{r} \beta_{mol}(r)dr}{\frac{X(r_c)}{\beta_{aer}(r_c)+\beta_{mol}(r_c)} - 2S_{aer}\{\int_{r_c}^{r} X(r)\ exp[-2(S_{aer} - S_{mol}) \int \beta_{mol}(r\prime)dr\prime]dr\}} \quad (5)$$

where $X(r)$ is the range normalized signal provided by $I(r)r^2$ and r_c is the reference height [19]. COD is calculated by integrating the extinction coefficient from cloud base to its top.

$$COD = \int_{Z_b}^{Z_t} \alpha(r)dr \quad (6)$$

where Z_t is the cloud top, Z_b is the cloud base, and $\alpha(r)$ is the extinction coefficient.

3.2. CALIPSO

The CALIPSO satellite was launched on 28 April 2006 and is an integral part of NASA's A-Train satellite constellation [20]. Its aim is to study the role that clouds and aerosols play in regulating the earth's weather, climate, and air quality. The main objectives of the CALIPSO are to (1) provide statistics on the vertical structure of clouds and aerosols around the globe, (2) detect sub-visible clouds in the upper troposphere and Polar Stratospheric Clouds (PSC), and (3) provide statistics on the geographic and vertical distribution of aerosols and clouds around the globe. The primary instrument aboard CALIPSO is the Cloud–Aerosol Lidar with Orthogonal Polarization (CALIOP), a two-wavelength laser (532 nm and 1064 nm) operating at a pulse repetition rate of 20.16 Hz [21]. Table 2 shows some specifications of CALIOP. More information on the technical specifications of CALIPSO can be found in Winker et al. [22] and Winker et al. [23]. Furthermore, Winker et al. [24] provide a detailed discussion on the algorithm that was developed to identify aerosol and cloud layers and to retrieve a variety of optical and microphysical properties.

Table 2. Specifications of CALIOP.

CALIOP Parameters	
Laser	Nd: YAG, diode-pumped, Q-switched, frequency doubled
Wavelengths	532 nm, 1064 nm
Pulse energy	110 mJ
Repetition rate	20.25 Hz
Receiver telescope	1.0 m diameter
Polarization	532 nm
Footprint/FOV	100 m/130 µrad
Vertical resolution	30–60 m
Horizontal resolution	333 m

4. Results and Discussion

In general, optical as well as microphysical properties of the cirrus clouds represent important but slightly incomplete information, especially if they are characterized in averaged values without considering temporal and spatial variation. The primary reason for this is that water vapor and ice particle concentrations vary within the cloud, usually as a nonlinear process. Due to the above-mentioned reason, as well as the current optical layout of the UZ lidar, the short-term variation of mean properties of the cirrus cloud is considered in this study. Furthermore, as mentioned earlier, the present study presents the case study of two cirrus cloud events that were captured at the beginning of the operation of the UZ lidar (10 and 11 April 2019). Figure 3a,b shows the temporal evolution of the total backscatter coefficients observed for the period from 17:42:12 pm to 20:16:25 on 10 April 2019. While there seems to be a signature indicating the presence of aerosols at a height below 2 km, there is a strong total backscatter coefficient between 9.5 and 11.5 km, which indicates the presence of a cirrus cloud. This is clearer in a zoomed-in version of Figure 3a, which is presented in Figure 3b. Over the detection time period, the cirrus cloud

is observed to propagate downwards, a characteristic that is similar to lidar observations presented by other studies. The calculation of the extinction coefficient using the successive signal returns for the 10 April 2019 also indicates a significant peak at ~2 km presumable due to an aerosol layer and a strong peak at ~10 km due to the presence of a cirrus cloud (see Figure 3b). COD was also estimated using Equation (6), and its time series is shown in Figure 3d. As displayed in this figure, the COD time series depicts a large variability on 10 April 2019, with increasing values up to above 1.7 during the first few minutes and in the middle of the times series, and minimum values which are less than 1.4 later in the time series. The average value of the COD is ~1.6. A study by Sassen and Cho [25] investigated a sub-visual-thin cirrus lidar dataset for the purpose of satellite data verification as well as climatological research. In this study, Sassen and Cho [25] suggested that cirrus clouds can be classified as thin cirrus with 0.03 < COD < 0.3, sub-visual cirrus with COD < 0.3, and dense cirrus with COD > 0.3. In this context, with an average value of COD which is way above 0.3 on 10 April 2019, the cirrus cloud observed here is a significant dense cirrus cloud.

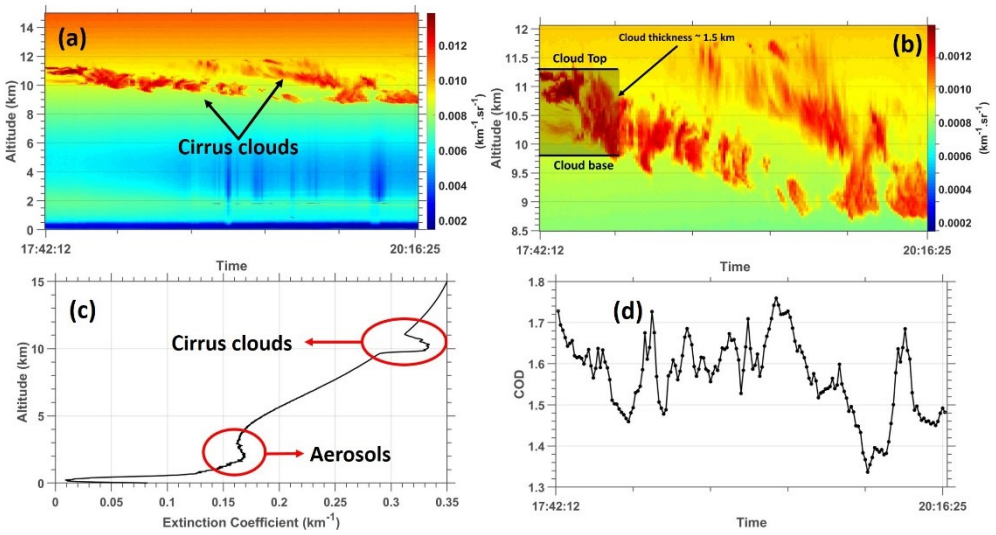

Figure 3. Height-time of total backscatter coefficients (**a**,**b**), extinction coefficient vs. altitude (**c**) and time evolution of cloud optical depth (COD) (**d**) for 10 April 2019.

A significant cirrus cloud was also observed over the study area on the succeeding day, 11 April 2019. It is worthy to also mention that the cirrus cloud seems to have disappeared in the days after 11 April 2019. Similar to Figure 3, Figure 4a shows the temporal evolution of the total backscatter coefficients observed for the period from 17:24:01 p.m. to 20:28:43 on 11 April 2019. Again, during this day, there seems to be a strong total backscatter coefficient peak at the height between 1 and 2 km, which is associated with the presence of aerosols in the lower troposphere over the study area. At the height between 9.5 and 11 km, a stronger total backscatter coefficient reaching a maximum value of 0.012 $km^{-1}sr^{-1}$ was observed. This approximately 1.5 km thick total backscatter coefficient peak is associated with a cirrus cloud which persists throughout the experiment duration. This cirrus cloud is classified as a dense cirrus cloud with COD values ranging from 1.48 to 1.70 (see Figure 4b). Unlike the cirrus cloud observed on 10 April 2019, the trend of the COD was observed to be upwards, with minimum values of approximately 1.48 at the beginning of the time series and maximum values of approximately 1.70 towards the end of the time series. The extinction coefficient vertical profile of the enhancement of the extinction coefficient at the height between 1 and 2 km and between 9.5 and 12 km due to the presence of aerosols and cirrus clouds, respectively (see Figure 4c,d).

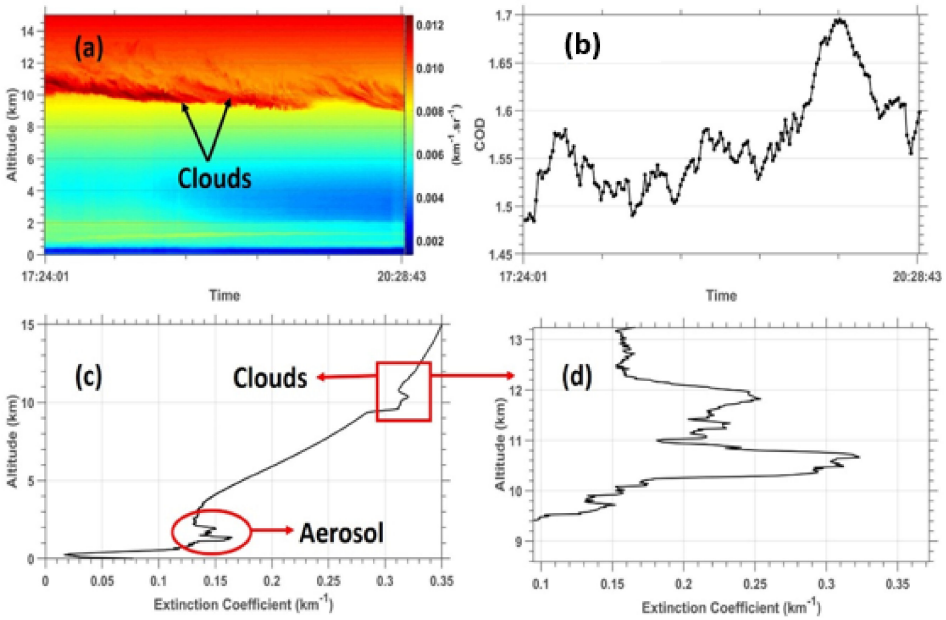

Figure 4. Height-time of total backscatter coefficients (**a**), time evolution of cloud optical depth (COD) (**b**), and extinction coefficient vs. altitude (**c**,**d**) for 11 April 2019.

The capabilities of the CALIPSO to measure clouds with an unprecedented vertical and horizontal resolution, especially high cloud, is an advantage for the characterization of cirrus clouds and the validation of ground-based lidar systems. The validation of the ground-based lidar largely depends on the availability of a CALIPSO closest overpass to the station of interest and also the days of the operation of the lidar. In this study, the closet CALIPSO overpass was only available on 11 April 2019. Figure 5a shows the total attenuated backscatter data at 532 nm for a section of CALIPSO's orbit on 11 April 2019. The CALIPSO cloud classification, as well as the vertical profile of the extinction coefficient as the satellite passes the closest to the UZ lidar locations, are shown in Figures 5b and 5c, respectively. The cloud type that is represented by a white color is a cirrus cloud. The orbit tract of CALIPSO is shown in Figure 5d. It is evident in Figure 5a that there is an enhancement of the total attenuated backscatter (<0.003 $km^{-1}sr^{-1}$) at the height region between 9 and 13 km. This strong peak was classified as a cirrus cloud (see Figure 5b). During this time, the CALIPSO satellite also reported a significant enhancement of the extinction coefficient vertical profile, which is directly associated with a cirrus cloud (see Figure 5c). This independent observation by the CALIPSO satellite agrees with the observation presented in Figure 4. The CALIPSO satellite observations also reported an ice and water content of about 0.009 gm^3 at around 10 km height.

The cirrus cloud events observed on both 10 and 11 April 2019 are very interesting because their COD is well above 1.0, thus indicating that the study area was dominated by dense cirrus clouds during this period. The optical depth of clouds is a crucial parameter concerning the radiation and scattering process of the cloud, and dense cirrus clouds events are less dominant in the atmosphere (e.g., Sivakumar et al. [2]). The variation of COD mainly depends on the thickness of the cloud [10] and density N of particles, and the mean particle size. In their study of cirrus clouds at two locations in the mid-latitudes of the southern (SH) and northern hemisphere (NH), Immler and Schrems [26] reported a frequent detection of haze layers of cirrus cloud in the NH and highly depolarizing cirrus cloud only in the SH. The average thickness of ~1.5 km of a cirrus cloud detected over a study area is within the range of what was reported by other authors such as Shikwambana and Sivakumar [10].

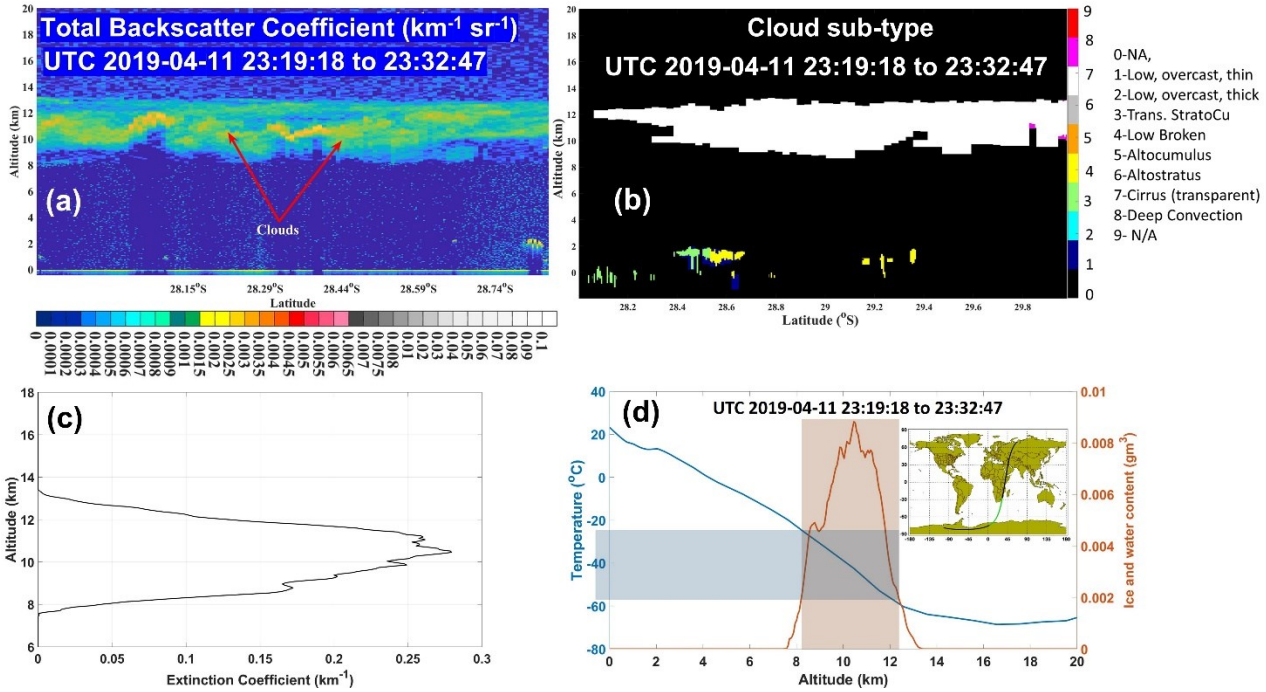

Figure 5. Height-time of (**a**) total backscatter coefficients, (**b**) cloud sub-type, (**c**) extinction coefficient for 11 April 2019. (**d**) Altitude vs ice and water content and temperature for 11 April 2019.

5. Conclusions

This study presents the characterization of cirrus clouds observed on 10 and 11 April 2019 using ground-based UZ lidar for the first time. The optical properties of cirrus clouds observed by the UZ lidar are also validated by using CALIPSO lidar closest overpass over the study area. This study reveals that a dense cirrus cloud with an average thickness of ~1.5 km at a height range of 9.5–12 km was observed by the UZ lidar on 10 and 11 April 2019. The availability of the closest overpass of CALISPO on 11 April 2019 allowed for the inter-comparison between the UZ lidar and the CALIPSO observations. A strong total backscatter coefficient peak at a height range of 8.5–12.5 km due to what was classified as a cirrus cloud was observed on 11 April 2019. Overall, there is a good agreement between the UZ lidar and CALIPSO instruments for cirrus cloud layer detection. It should also be mentioned here that the UZ lidar is able to detect aerosols at the lower troposphere, a feature that is also apparent in the CALISPO observations. A study on the long-term characterization of cirrus clouds and the frequency occurrence, as well as aerosols, will follow as soon as enough UZ lidar data are available.

Author Contributions: Conceptualization, N.M. and L.S.; methodology, N.M. and L.S.; software, N.M.; validation, N.M. and L.S.; formal analysis, N.M. and L.S.; investigation, N.M.; writing—original draft preparation, L.S.; writing—review and editing, N.M. All authors have read and agreed to the published version of the manuscript.

Funding: The APC was funded by the University of Zululand.

Institutional Review Board Statement: Not applicable.

Informed Consent Statement: Not applicable.

Data Availability Statement: The datasets generated during and/or analysed during the current study are available from the corresponding author on reasonable request. CALIPSO dataset can be accessed on https://search.earthdata.nasa.gov/ (accessed on 2 February 2022).

Acknowledgments: This project is sponsored by the CSIR NLC Rental Pool Programme. Authors acknowledge the French South-African PROTEA programme and the CNRS-NRF LIA ARSAIO (Atmospheric Research in Southern Africa and Indian Ocean), for supporting research activities,

and the National Research Foundation (NRF) of South Africa. A special thanks to Sivakumar Venkataraman for his assistance during the first phase of the operation of the instrument. We thank the Atmospheric Science Data Center at NASA Langley Research Center for archiving and hosting CALIPSO data.

Conflicts of Interest: The authors declare no conflict of interest.

References

1. Liou, K.N. Influence of cirrus clouds on weather and climate processes: A global perspective. *Mon. Weather Rev.* **1986**, *114*, 1167–1199. [CrossRef]
2. Sivakumar, V.; Bhavanikumar, Y.; Rao, P.B.; Mizutani, K.; Aoki, T.; Yasui, M.; Itabe, T. Lidar observed characteristics of the tropical cirrus clouds. *Radio sci.* **2003**, *38*, 1094. [CrossRef]
3. Nicolas, J.P.; Bromwich, D.H. Climate of West Antarctica and influence of marine air intrusions. *J. Clim.* **2011**, *24*, 49–67. [CrossRef]
4. Qian, Y.; Long, C.N.; Wang, H.; Comstock, J.M.; McFarlane, S.A.; Xie, S. Evaluation of cloud fraction and its radiative effect simulated by IPCC AR4 global models against ARM surface observations. *Atmos. Chem. Phys.* **2012**, *12*, 1785–1810. [CrossRef]
5. Zhou, C.; Zelinka, M.D.; Klein, S.A. Analyzing the dependence of global cloud feedback on the spatial pattern of sea surface temperature change with a Green's function approach. *J. Adv. Model Earth Syst.* **2017**, *9*, 2174–2189. [CrossRef]
6. Stubenrauch, C.J.; Rossow, W.B.; Kinne, S.; Ackerman, S.; Cesana, G.; Chepfer, H.; Di Girolamo, L.; Getzewich, B.; Guignard, A.; Heidinger, A.; et al. Assessment of Global Cloud Datasets from Satellites: Project and Database Initiated by the GEWEX Radiation Panel. *Bull. Am. Meteorol. Soc.* **2013**, *94*, 1031–1049. [CrossRef]
7. Karlsson, K.-G.; Dybbroe, A. Evaluation of arctic cloud products from the EUMETSAT climate monitoring satellite application facility based on CALIPSO-CALIOP observations. *Atmos. Chem. Phys.* **2010**, *10*, 1789–1807. [CrossRef]
8. Ansmann, A.; Riebesell, M.; Wandinger, U.; Weitkamp, C.; Voss, E.; Lahmann, W.; Michaelis, W. Combined Raman elastic-backscatter LIDAR for vertical profiling of moisture, aerosol extinction, backscatter, and LIDAR ratio. *Appl. Phys.* **1992**, *B55*, 18–28. [CrossRef]
9. Sassen, K.; Griffin, M.; Dood, G.C. Optical scattering and microphysical properties of subvisible cirrus clouds, and climatic implications. *J. Appl. Meteorol.* **1989**, *28*, 91–98. [CrossRef]
10. Shikwambana, L.; Sivakumar, V. Observation of Clouds Using the CSIR Transportable LIDAR: A Case Study over Durban, South Africa. *Adv. Meteorol.* **2016**, *2016*, 4184512. [CrossRef]
11. Wang, Z.; Shishko, V.A.; Konoshonkin, A.V.; Kustova, N.V.; Borovoi, A.G.; Matvienko, G.G.; Xie, C.; Liu, D.; Wang, Y. The study of cirrus clouds with the polarization lidar in the South-East China (Hefei). *Atmos. Ocean. Opt.* **2017**, *30*, 234–235. [CrossRef]
12. Okello, N.O.; Okello, T.W.; Zuncke, M. Public perceptions of air quality status and suggestions for improvement: The case of Richards Bay and its surroundings, Mhlathuze Local Municipality, South Africa. *Clean Air J.* **2020**, *30*, 1–10. [CrossRef]
13. Comerón, A.; Muñoz-Porcar, C.; Rocadenbosch, F.; Rodríguez-Gómez, A.; Sicard, M. Current Research in Lidar Technology Used for the Remote Sensing of Atmospheric Aerosols. *Sensors* **2017**, *17*, 1450. [CrossRef] [PubMed]
14. Winker, D.M.; Pelon, J.; Coakley, J.A.; Ackerman, S.A.; Charlson, R.J.; Colarco, P.R.; Flamant, P.; Fu, Q.; Hoff, R.M.; Kittaka, C.; et al. The CALIPSO mission: A global 3D view of aerosols and clouds. *Bull. Am. Meteorol. Soc.* **2010**, *91*, 1211–1229. [CrossRef]
15. Nellore, M.K.; Kannan, V. Lidar Observed Optical Properties of Tropical Cirrus Clouds Over Gadanki Region. *Front. Earth Sci.* **2020**, *8*, 140. [CrossRef]
16. Kottek, M.; Grieser, J.; Beck, C.; Rudolf, B.; Rubel, F. World map of the Köppen-Geiger climate classification updated. *Meteorol. Zeitschrift* **2006**, *15*, 259–263. [CrossRef]
17. Sharma, A.; Sivakumar, V.; Bollig, C.; van der Westhuizen, C.; Moema, D. System description of the mobile LIDAR of the CSIR, South Africa. *South Afr. J. Sci.* **2009**, *105*, 456–462. [CrossRef]
18. Klett, J.D. Stable analytical inversion solution for processing lidar returns. *Appl. Opt.* **1981**, *20*, 211–220. [CrossRef]
19. Fernald, F.G. Analysis of atmospheric lidar observations: Some comments. *Appl. Opt.* **1984**, *23*, 652–653. [CrossRef]
20. Stephens, G.L.; Vane, D.G.; Boain, R.J.; Mace, G.G.; Sassen, K.; Wang, Z.; Illingworth, A.J.; O'Connor, E.J.; Rossow, W.B.; Durden, S.L.; et al. The CloudSat mission and the A-Train: A new dimension of space-based observations of clouds and precipitation. *Bull. Am. Meteorol. Soc.* **2002**, *83*, 1771–1790. [CrossRef]
21. Hunt, W.H.; Winker, D.M.; Vaughan, M.A.; Powell, K.A.; Lucker, P.L.; Weimer, C. CALIPSO Lidar Description and Performance Assessment. *J. Atmos. Ocean Technol.* **2009**, *26*, 1214–1228. [CrossRef]
22. Winker, D.M.; Pelon, J.; McCormick, M.P. The CALIPSO mission: Spaceborne lidar for observation of aerosols and clouds. In Proceedings of the Volume 4893, Lidar Remote Sensing for Industry and Environment Monitoring III, Hangzhou, China, 8 May 2003. [CrossRef]
23. Winker, D.M.; Tackett, J.L.; Getzewich, B.J.; Liu, Z.; Vaughan, M.A.; Rogers, R.R. The global 3-D distribution of tropospheric aerosols as characterized by CALIOP. *Atmos. Chem. Phys.* **2013**, *13*, 3345–3361. [CrossRef]
24. Winker, D.M.; Vaughan, M.A.; Omar, A.; Hu, Y.; Powell, K. Overview of the CALIPSO Mission and CALIOP Data Processing Algorithms. *J. Atmos. Ocean Technol.* **2009**, *26*, 2310–2323. [CrossRef]

25. Sassen, K.; Cho, B.S. Subvisual-Thin Cirrus Lidar Dataset for Satellite Verification and Climatological Research. *J. Appl. Meteorol. Climatol.* **1992**, *31*, 1275–1285. [CrossRef]
26. Immler, F.; Schrems, O. LIDAR measurements of cirrus clouds in the northern and southern midlatitudes during INCA (55°N, 53°S): A comparative study. *Geophys. Res. Lett.* **2002**, *29*, 6389. [CrossRef]